Energy- and exergy-based optimal designs of a low-temperature industrial waste heat recovery system in district heating

Jaume Fito, Sacha Hodencq, Julien Ramousse, Frederic Wurtz, Benoit Stutz, François Debray, Benjamin Vincent

Energy- and exergy-based optimal designs of a low-temperature industrial waste heat recovery system in district heating

Jaume Fitó[a], Sacha Hodencq[b], Julien Ramousse[a,], Frédéric Wurtz[b], Benoit Stutz[a], François Debray[c], Benjamin Vincent[c]*

[a] *Laboratoire Optimisation de la Conception et Ingénierie de l'Environnement (LOCIE), CNRS UMR 5271 – Université Savoie Mont Blanc, Polytech Annecy-Chambéry, Campus Scientifique, Savoie Technolac, 73376 Le Bourget-Du-Lac Cedex, France*

[b] *Univ. Grenoble Alpes, CNRS, Grenoble INP (Institute of Engineering Univ. Grenoble Alpes), G2Elab, 38000 Grenoble, France*

[c] *Laboratoire National des Champs Magnétiques Intenses (LNCMI), CNRS-UPS-INSA-UJF, 25 Rue des Martyrs, 38042 Grenoble, France*

** Corresponding author: J. Ramousse.*

Abstract

This paper illustrates how the choice of indicators changes the design of a waste heat recovery system in district heating. A prospective system in Grenoble (France) aims to valorize waste heat from the French National Laboratory of Intense Magnetic Fields (LNCMI) by injecting it at 85 °C to the nearby district heating network. We optimize its design for three possible waste heat temperatures: 35 °C (current), 50 °C (viable) and 85 °C (innovative). As major components, the system includes a thermal storage (ranging from 10 MWh to 40 MWh) and may include a heat pump depending on the waste heat's temperature. Different optimizations are guided by two energetic indicators (one source-oriented, the other demand-oriented) and by the overall exergy efficiency. The system's annual performance is assessed through the Sankey and Grassman diagrams and compared between optimal designs. Yearly simulation included optimal management of the thermal storage, through mixed-integer linear programming. The demand-oriented optimal design suggests recovering waste heat at 35 °C with a heat pump and a 40-MWh storage, granting the highest coverage of residential needs (49 %). On the other hand, the source-oriented optimal design suggests recovering waste heat at 85 °C without heat pump and with a 40-MWh storage, reaching the highest recovery of waste heat (55 %). Exergy analysis supports the source-oriented design, as it reaches the highest global exergy efficiency (27 %). Our prospective techno-economic and exergo-economic analyses should complement these results and may change some conclusions, especially regarding the storage capacity.

Keywords

Waste heat recovery, District heating network, Design optimization, Energy management, Exergy optimization.

Highlights

- Energy-based (source- or demand-oriented) and exergy-based optimal designs differ.
- Source-oriented energy-optimal design reaches highest waste heat recovery (55 %).
- Demand-oriented energy-optimal design reaches highest demand coverage (49 %).
- Exergy analysis supports source-oriented optimum (27 % global exergy efficiency).
- Main discrepancy between indicators revolves around using or not using a heat pump.

Nomenclature

Names and Variables		GLOB	Global
COP	Coefficient Of Performance	HP	Heat pump
ex	Specific exergy (kJ/kg)	HS	Heat supplier
Ex	Exergy [kWh or GWh]	in	Inlet
$\dot{E}x$	Exergy rate (kW)	ini	Initial
$\dot{m}$	Mass flow rate (kg/s)	L	Total loss
P	Pressure (bar)	l	Losses
Q	Heat (kWh, MWh or GWh)	LNCMI	Laboratoire National des Champs Magnétiques Intenses
$\dot{Q}$	Thermal power (kW)	max	Maximal
T	Temperature (°C)	min	Minimal
t	Time [h]	SST	Network sub-stations
$\dot{W}$	Power (kW)	sup	Network's supply
		ret	Network's return
Subscripts and Superscripts		TES	Thermal Energy Storage
C	Carnot cycle	th	Thermal
D	Destruction	W	Work
DHN	District Heating Network	wh	Waste heat
DISS	Dissipation	WHRS	Waste Heat Recovery System
el	Electrical		
out	Outlet	***Greek Symbols***	
Q	Heat	η	Efficiency (%)
f	Final	ξ	Electricity-to-heat conversion ratio [kW_{th}/kW_{el}]

1. Introduction

As district heating networks evolve, the integration of low-temperature heat sources has become increasingly feasible and interesting. This is especially true for advanced district heating systems (i.e. 4th generation onwards) [1]. Studies in the literature have pointed out the interest of integrating industrial waste heat [2,3] or other waste sources capable of producing heat [4] into district heating systems.

The diversity of sources, types of energy and temperature levels can make energy analysis insufficient. First-law analysis and energetic indicators alone fail to account for the quality of energy streams in a system [5]. For instance, the Coefficient of Performance (COP) of a heat pump is misleading, because it attributes the same thermodynamic value to both work and heat transfer [6]. Furthermore, while energy balance allows to calculate heat losses, it cannot give information on how to optimally transform energy [7]. On the other hand, exergy does adjust the value of energy depending on its quality. In addition, this magnitude has the same units as energy, which makes it easier to apply and interpret than entropy.

Thanks to its advantages, exergy is increasingly used in district heating analysis [8]. For example, it has been suggested as a criterion for a more sustainable urban development [9,10]. It has also been suggested for detecting nearby low-temperature sources for integration, an approach called “low-exergy urban planning” [11]. It has even been suggested as main criterion for control strategies, with encouraging results in building energy systems [5] and in geothermal district heating [12]. When waste heat is considered for district heating, exergy analysis determines the quality matching between the low-temperature waste heat and the low-grade residential demands [13].

Investigations based on mixed electric-thermal models are emerging specially in countries where heat districts are historically developed, for instance in eastern and northern Europe [1]. These kinds of studies usually imply the use of an exergetic approach and sometimes require multi-objective optimization too [14].

In this article, we present a case study of industrial low-temperature waste heat recovery for valorization in the local district heating network. The case presents an intermittent profile of low-temperature waste heat rejection, and a variable profile of residential heat demand. These profiles are mismatched, and in addition, the temperature of the waste heat is insufficient for direct injection into the district heating network. To address the issue of heat recovery, a system consisting of a thermal energy storage and a heat pump is proposed. Several possibilities of storage capacity and waste heat temperature are also investigated. The fact that this case study involves energies of different quality and heat flows of different temperatures made it suitable for exergetic analysis. In all scenarios, the energy-oriented optimization and the exergy-oriented optimization were compared.

2. Methodology

2.1. System description

Fig. 1 is what the authors call the “exergo-diagram” of the study case. Similar types of figures exist in the literature that organize potential heat sources according to their temperature levels [11]. The figure presented here just takes the concept a bit further and uses the exergy factor as classification tool, thus allowing to compare different energy vectors. The higher the exergy factor (quality) of an energy flow, the further up its position within the y-axis. Consequently, electricity is at the highest position, followed by thermal energy in a descending order, as function of its temperature. As an additional advantage, this kind of figure facilitates an intuitive perception of the exergy destruction within each unit. In Fig. 1, continuous and dashed lines respectively represent the existing and prospective systems.

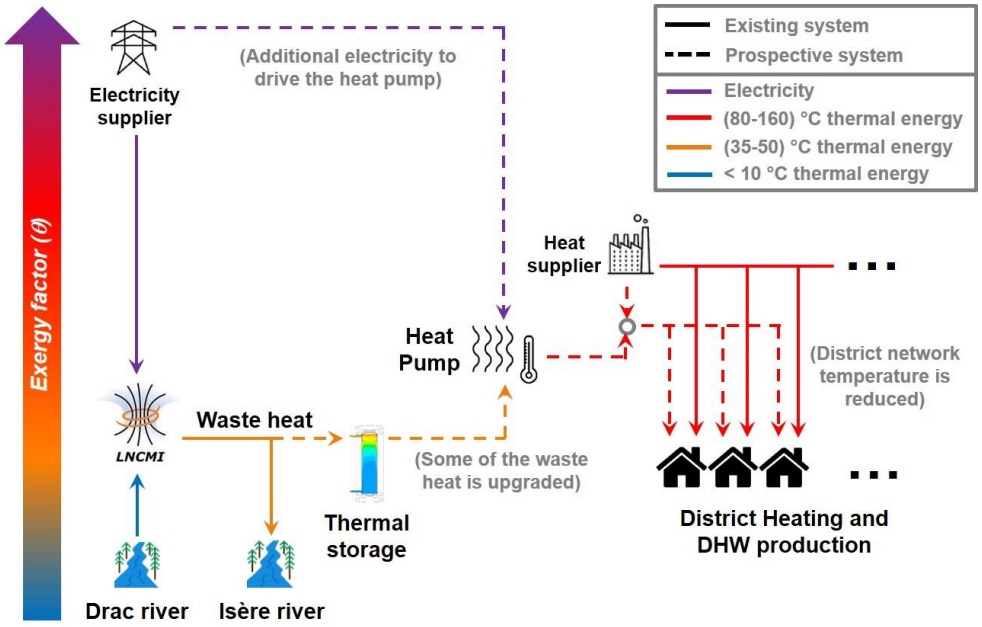

Figure 1. Exergo-diagram of the existing and prospective systems for the LNCMI waste heat recovery.

The *Laboratoire National des Champs Magnétiques Intenses* of Grenoble (LNCMI for the French National High Magnetic Field Laboratory) is a research facility of the French National Centre for Scientific Research (CNRS). It provides researchers and engineers from all over the world with high magnetic fields. Electro-magnets consume electricity to produce high-intensity magnetic fields, which in turn produce invaluable results for scientific research. The LNCMI was characterized in 2018 by a total electricity consumption of 21 GWh for 24 MW of installed capacity (Fig. 2). This profile highlights the high intermittency and the sharp peaks of the electricity consumption. The magnetic field does not work, so all the electrical energy injected into these magnets is dissipated as heat due to the Joule effect. A hydraulic circuit uses cold water from the nearby Drac river to extract (through an exchanger)

calories from the magnets' closed cooling circuit. Then, it discharges the hot water into the Isère river. The outlet temperature of the magnets depends on the magnet power, the Drac river temperature and the cooling mode. It varies between 10 ˚C and 40 ˚C along the year, usually around 35 ˚C.

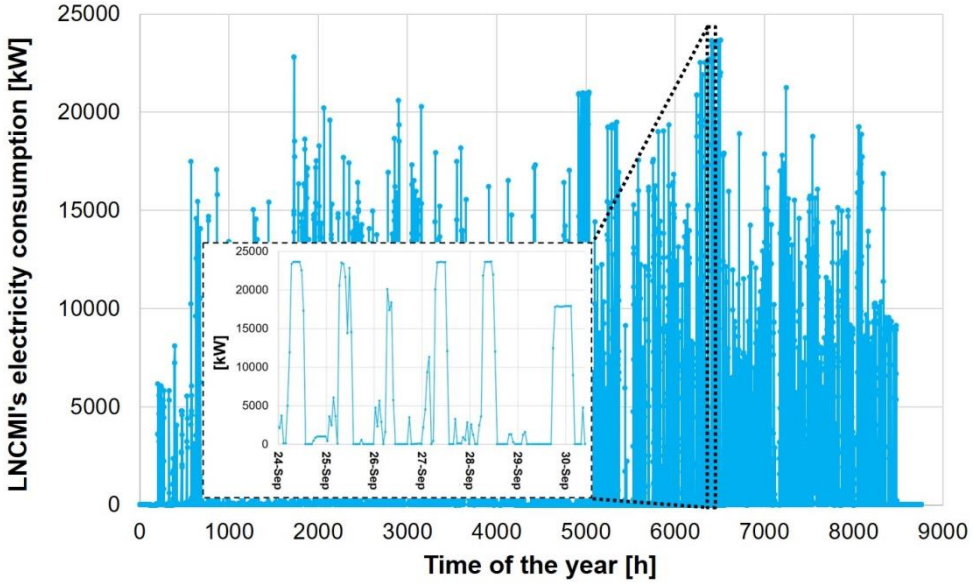

Figure 2. Hourly profile of electric power consumption by the LNCMI (full year + zoom into one week).

Not far from the LNCMI, a large district heating network is meant to cover the need for residential heating and domestic hot water in the Presqu'île district of Grenoble. Currently, the inlet temperature of this network is at 120 °C, although its operator plans to reduce it to 85 °C in the near future. The study presented in this paper works with the hypothesis that the district heating network will be at 85 °C.

Fig. 3 shows the thermal power tranches of both the LNCMI's waste heat and the district heating network's demands. The residential annual hourly profile is subjected to confidentiality constraints, but is similar to typical residential needs [15]. Both the annual electricity consumption and the instantaneous electric power for the LNCMI's experiences are abundant. The total waste heat from these experiences is theoretically sufficient to cover a large portion of the residential demands. This is an interesting opportunity to evaluate the potential of a heat recovery and valorization system. Such a system needs to assess two major challenges. First, the temporal mismatch [16] between waste heat rejection and residential demand. Second, the fact that the waste heat temperature is currently too low for direct injection into the district heating network.

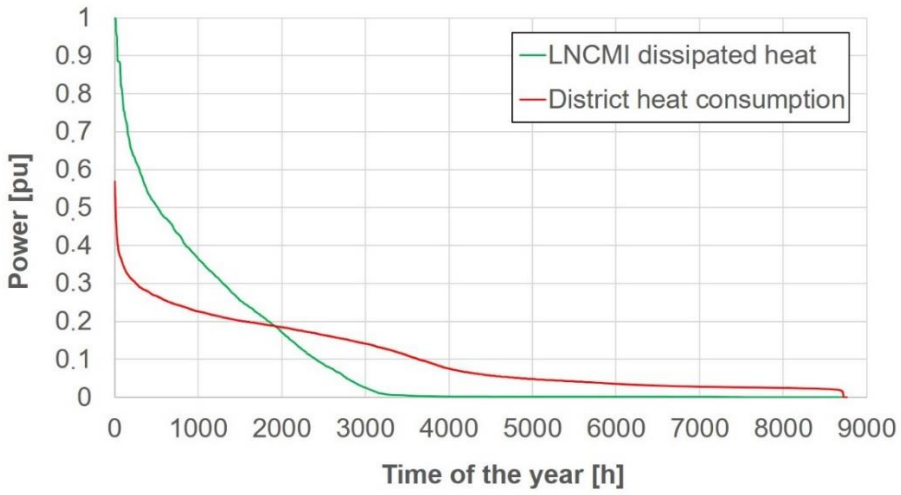

Figure 3. Power tranches of the LNCMI's magnets and the district heating network consumption.

The Waste Heat Recovery System (WHRS) proposed to answer these challenges (Fig. 4) is made up of a thermocline energy storage (TES) unit [17,18] and a conventional, electrically-driven water/water heat pump (HP). The heat pump is essential for upgrading the waste heat to a temperature of 85 °C, which is the minimal supply temperature of the district heating network. The thermocline storage is selected because of its high reliability and Technology Readiness Level (TRL). The storage is essential for evening out the LNCMI heat production peaks and compensating the short-term mismatch between the waste heat rejection and the network's heat consumption. Given the profiles, long-term or seasonal storage is not required for this studied case. As shown in Fig. 3, the waste heat and the residential needs are similar amounts. Therefore, with the proper sizing and control strategy, the valorization system could be able to cover the entire demands with the waste heat only. Besides, the maximum charging/discharging powers are insufficient to absorb the power peaks coming from the LNCMI.

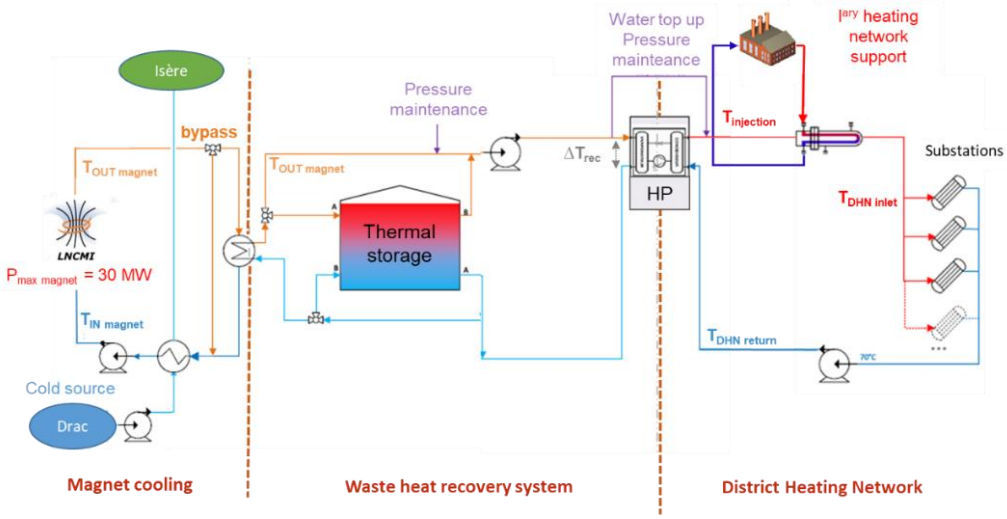

Figure 4. Detailed technical diagram of the overall prospective system.

There are three main scenarios and several cases for each scenario, depending on the temperature of the waste heat and the storage capacity. The first main case, called “Reference case”, corresponds to an absence of waste heat recovery, which is the current situation for the LNCMI. This reference case was evaluated at three different temperatures for the waste heat: 35 ˚C, 50 ˚C and 85 ˚C. The cooling loop can be regulated for a consistent 35 ˚C outlet temperature, and is theoretically adjustable to reject at higher temperatures. This adjustment is currently under study by the engineering team of the LNCMI.

The second main case consists in heat valorization with the waste heat being at a lower temperature (i.e. 35 ˚C or 50 ˚C) than the network’s minimum requirements. This case requires the heat pump, and it was evaluated for different storage capacities. The scenario with a storage capacity of 0 MWh means that heat is only valorized when the waste heat and the residential demands are simultaneous.

The third and final main case consists of heat valorization when the waste heat is at 85 ˚C. This temperature is theoretically possible if the LNCMI’s magnets are cooled down by means of nucleate boiling [19]. This case differs from the previous ones in that no heat pump is needed. Again, several storage capacities were considered.

The current studies on this case apply a first-law approach and are focused on mismatch compensation by means of storage and management of the thermal energy flows. Nevertheless, the energy balances applied on some of the units imply both electrical and thermal energy without accounting for their quality. Furthermore, temperature levels of the thermal flows are not taken into account either. These two shortcomings of the first-law approach made the exergetic analysis interesting for all the partners involved in the project. One of the objectives of the study presented in this paper is to find out whether exergy analysis can identify a management strategy missed by energy analysis.

2.2. Optimization tool and procedure

For the optimization, the tool OMEGAlpes was used [20,21]. It anticipates the management of energy flows [22] by means of mixed-integer linear programming (MILP), an approach sometimes applied to district heating [23,24]. OMEGAlpes is a linear optimization tool designed to generate multi-carrier energy system models easily. Its purpose is to assist in the modelling of energy system for pre-studies integrating design and operation. OMEGAlpes is developed by the Grenoble Electrical Engineering Laboratory (G2Elab, France) in open-source and written in Python. The tool provides a high abstraction environment: the multi-energy system of the LNCMI is modeled as various production, consumption, storage and conversion units, connected together through energy

nodes. A time unit is set, as well as constraints and an objective. The python script used to model this case study is available at the Examples repository [25] of OMEGAlpes' documentation [26].

2.3. Energy analysis

Given the transient nature of residential demands, and the intermittence of waste heat, energy balances in this study are done on an annual basis with an hourly time step. The following working hypotheses were used:

- Pressure, temperature and heat losses across all pipelines are neglected.
- Temperature losses inside the thermal energy storage were not considered.
- The initial and final state of charge of the thermal energy storage are the same.
- Heat losses within the heat pump are neglected.

For the LNCMI, waste heat rejection is straightforwardly calculated by means of a conversion factor from electrical energy to thermal energy (eq. 1) corresponding to the ratio between the heat dissipated in the resistive electro-magnets and the electricity consumed by the LNCMI facility. The waste heat can then be dissipated, sent directly to the heat pump (or to the DHN when T_{wh} = 85 ˚C), or stored for later usage (eq. 2).

$$\dot{Q}_{wh}(t) = \xi \cdot \dot{W}^{el}_{LNCMI}(t) \tag{1}$$

$$\dot{Q}_{wh}(t) = \dot{Q}_{DISS}(t) + \dot{Q}'^{in}_{HP}(t) + \dot{Q}^{in}_{TES}(t) \tag{2}$$

As mentioned in the case description, the recovery system includes a non-pressurized thermocline storage of water. The storage's inlet or outlet energy flow is limited, respectively, by the maximum charging or discharging power corresponding to one third of the total capacity (eqs. 3 and 4). The charging/discharging time is assumed to be 3 hours, which is around the typical values reported in the literature [27,28]. The heat contained at the next time step is calculated through the energy balance at the current time step (eq. 5). Heat losses close to 1 %/day were reported in [28] for a storage containing heat at 35 ˚C with its surroundings being at 20 ˚C. For the scenarios at 50 ˚C and 85 ˚C, these losses were re-evaluated as a function of the temperature difference between the storage and the environment. The adjusted values are 2 %/day at 50 ˚C and 4.3 %/day at 85 ˚C. The heat contained cannot fall below zero or exceed the maximum capacity (eq. 6). In addition, the initial and final states of charge must be the same (eq. 7).

$$\dot{Q}^{in}_{TES}(t) \leq \dot{Q}^{in,max}_{TES} \tag{3}$$

$$\dot{Q}^{out}_{TES}(t) \leq \dot{Q}^{out,max}_{TES} \tag{4}$$

$$Q_{TES}(t + \Delta t) = Q_{TES}(t) + \dot{Q}^{in}_{TES}(t) - \dot{Q}^{out}_{TES}(t) - \dot{Q}^{l}_{TES}(t) \tag{5}$$

$$0 \leq Q_{TES}(t) \leq Q_{TES}^{max} \quad (6)$$

$$Q_{TES}(t_f) = Q_{TES}(t_{ini}) \quad (7)$$

The input heat to the heat pump can come either from the storage unit ($\dot{Q}_{TES}^{out}(t)$), or directly from LNCMI's experiments ($\dot{Q}'^{in}_{HP}(t)$) that are simultaneous with the residential needs (eq. 8). An energy balance is applied on the heat pump (eq. 9), having its COP into account (eq. 10). The value of COP_{HP} at T_{HP}^{in} = T_{wh} = 35 ˚C corresponds to a real heat pump, while the value of COP_{HP} at T_{HP}^{in} = T_{wh} = 50 ˚C corresponds to an extrapolation of the real heat pump by assuming that its second-law efficiency stays the same (eq. 11), with constant maximum outlet thermal power.

$$\dot{Q}_{HP}^{in}(t) = \dot{Q}'^{in}_{HP}(t) + \dot{Q}_{TES}^{out}(t) \quad (8)$$

$$\dot{Q}_{HP}^{in}(t) + \dot{W}_{HP}^{el}(t) = \dot{Q}_{HP}^{out}(t) \quad (9)$$

$$COP_{HP} = \frac{\dot{Q}_{HP}^{out}(t)}{\dot{W}_{HP}^{el}(t)} \quad (10)$$

$$\frac{COP_{HP}\left(T_{HP}^{in}=50\,°C\right)}{COP_{C}\left(T_{HP}^{in}=50\,°C\right)} = \frac{COP_{HP}\left(T_{HP}^{in}=35\,°C\right)}{COP_{C}\left(T_{HP}^{in}=35\,°C\right)} \quad (11)$$

The total amount of heat supplied to the DHN is the sum of the contributions from the heat supplier and the valorization system (eq. 12). It is assumed that the heat supplier is capable, at any time, of covering all the residential demands that are not being covered by the WHRS. The output thermal power of the WHRS depends on whether the waste heat temperature is 85 °C (eq. 13) or not (eq. 14).

$$\dot{Q}_{WHRS}^{out}(t) + \dot{Q}_{HS}(t) = \dot{Q}_{DHN}^{sup}(t) \quad (12)$$

$$\dot{Q}_{WHRS}^{out}(t) = \dot{Q}_{wh}(t) - \dot{Q}_{DISS}(t) - \dot{Q}_{TES}^{l}(t) \qquad if\ T_{wh} = 85\,°C \quad (13)$$

$$\dot{Q}_{WHRS}^{out}(t) = \dot{Q}_{HP}^{out}(t) \qquad if\ T_{wh} = 35\,°C\ or\ 50\,°C \quad (14)$$

One of the two criteria used for the energetic optimization is the Recovery Factor (*RF*, eq. 15). This indicator accounts for the total intake of waste heat by the WHRS, in relation to the total waste heat available. Similar indicators exist in the literature, for instance to evaluate how much energy of a renewable source has been utilized [29].

$$Recovery\ Factor\ (RF) = \frac{\sum_{t=t_{ini}}^{t=t_f} \dot{Q}_{HP}^{in}(t) \cdot \Delta t}{\sum_{t=t_{ini}}^{t=t_f} \dot{Q}_{wh}(t) \cdot \Delta t} \cdot 100 \quad (15)$$

In addition to the total recovery of waste heat, it is also interesting to evaluate the share of residential demand that is covered by the WHRS. To this purpose, the Coverage Factor (*CF*, eq. 16) was defined. Again, similar types of indicators are used in the literature when intermittent energy sources are considered [16]. The fundamental difference between this indicator and the *RF* is that while the *RF* is source-oriented, the *CF* is demand-oriented. Table 1 introduces the values used for all parameters and variables used in the energy model.

$$Coverage\ Factor\ (CF) = \frac{\sum_{t=t_{ini}}^{t=t_f} \dot{Q}_{WHRS}^{out}(t) \cdot \Delta t}{\sum_{t=t_{ini}}^{t=t_f} \dot{Q}_{DHN}^{sup}(t) \cdot \Delta t} \cdot 100 \quad (16)$$

Table 1. Magnitudes used for the energy model.

Magnitude	Type	Value(s) or limit(s)	Units
Δt	Fixed parameter	1	[h]
ξ	Fixed parameter	0.85	[kW_{th} / kW_{el}]
$COP_{HP}\left(T_{HP}^{in} = 35\ °C\right)$	Fixed parameter	3	[kW_{th} / kW_{el}]
$COP_{HP}\left(T_{HP}^{in} = 50\ °C\right)$	Fixed parameter	4.29	[kW_{th} / kW_{el}]
$\dot{Q}_{TES}^{in,max}$	Fixed parameter	$= {Q_{TES}^{max}}/{3}$	[MW]
$\dot{Q}_{TES}^{out,max}$	Fixed parameter	$= {Q_{TES}^{max}}/{3}$	[MW]
t_{ini}	Fixed parameter	0	[h]
t_f	Fixed parameter	8760	[h]
T_{HP}^{in}	Fixed parameter	[35, 50]	[°C]
T_{HP}^{out}	Fixed parameter	85	[°C]
T_{HS}	Fixed parameter	120	[°C]
$\dot{W}_{HP}^{el,max}\left(T_{HP}^{in} = 35\ °C\right)$	Fixed parameter	1260	[kW_{el}]
$\dot{W}_{HP}^{el,max}\left(T_{HP}^{in} = 50\ °C\right)$	Fixed parameter	881	[kW_{el}]
Q_{TES}^{max}	Optimization parameter	[0, 10, 20, 30, 40]	[MWh]
T_{wh}	Optimization parameter	[35, 50, 85]	[°C]
CF	Optimization criterion	[0 – 100]	[% ; kW_{th} / kW_{th}]
RF	Optimization criterion	[0 – 100]	[% ; kW_{th} / kW_{th}]

2.4. Exergy analysis

The exergy analysis is built on the energy analysis by adding new variables, parameters and balances. Most of the new information refers to the temperatures of the thermal flows and the exergetic efficiency of some units. In addition to the hypotheses from the energy model, the following hypotheses were added:

- Potential and kinetic exergy are neglected.
- The heat production process by the heat supplier has a constant exergetic efficiency ($\eta_{ex,HS}$).

- Exergy destruction within the LNCMI is dismissed, since the main useful effect delivered by this unit is not quantifiable for exergy analysis. As stated in the introduction, the LNCMI provides researchers with invaluable experimental data, while the waste heat is just a by-product of its activities.

Since all the heat received by the Isère river is dissipated, it was entirely assumed as an exergy destruction (eq. 17). Although the Isère's temperature fluctuates over the year, the value of T_0 was kept constant (at T_0 = 8 ˚C), for the sake of thermodynamic consistency [30].

$$\dot{Ex}^D_{DISS}(t) = \dot{Q}_{DISS}(t) \cdot \left(1 - \frac{T_0}{T_{wh}}\right) \quad (17)$$

With the hypotheses used in the model there is no exergy destruction within the TES unit itself. However, this unit does have some heat losses, which imply exergy losses (eq. 18).

$$\dot{Ex}^l_{TES}(t) = \dot{Q}^l_{TES}(t) \cdot \left(1 - \frac{T_0}{T_{TES}}\right) \quad (18)$$

Exergy destruction within the heat pump results from applying the exergy balance (eq. 19).

$$\dot{Ex}^D_{HP}(t) = \dot{Q}^{in}_{HP}(t) \cdot \left(1 - \frac{T_0}{T_{\dot{Q}^{in}_{HP}}}\right) + \dot{W}^{el}_{HP}(t) - \dot{Q}^{out}_{HP}(t) \cdot \left(1 - \frac{T_0}{T_{\dot{Q}^{out}_{HP}}}\right) \quad (19)$$

The exergy destruction within the heat supplier unit was calculated assuming that its process has a constant exergy efficiency (eq. 20). Currently, the heat supplier obtains its primary energy from a mix of renewable and non-renewable sources. 36.9 % of it comes from household waste, 29 % from wood, 16.7 % from coal, 7.6 % from natural gas, 6.2 % from industrial exhaust heat, 2.5 % from biomass, 1 % from fuels oil, and 0.1 % from liquid biofuels. An exergy efficiency of η^{ex}_{HS} = 0.40 was assumed for their combustion process. This value is around typical exergy efficiencies for natural gas-fired boilers [31] or steam boilers [32].

$$\dot{Ex}^D_{HS}(t) = \dot{Q}_{HS}(t) \cdot \left(1 - \frac{T_0}{T_{HS}}\right) \cdot \left(\frac{1}{\eta^{ex}_{HS}} - 1\right) \quad (20)$$

Exergy destruction within the district heating network (DHN) was calculated as the difference between the inlet contributions (i.e. the heat pump and the heat supplier) and the exergy at the network's supply (eq. 21). Since in all scenarios $T_{out,HP} = T_{sup,DHN} = 85\,°C$, the only exergy destruction comes from reducing the supplier heat's temperature from 120 ˚C to 85 ˚C. Therefore, equation 21 can be rearranged as equation 22.

$$\dot{Ex}^D_{DHN}(t) = \dot{Q}^{out}_{HP}(t) \cdot \left(1 - \frac{T_0}{T^{out}_{HP}}\right) + \dot{Q}_{HS}(t) \cdot \left(1 - \frac{T_0}{T_{HS}}\right) - \dot{Q}^{sup}_{DHN}(t) \cdot \left(1 - \frac{T_0}{T^{sup}_{DHN}}\right) \quad (21)$$

$$\dot{Ex}^D_{DHN}(t) = \dot{Q}_{HS}(t) \cdot \left(\frac{T_0}{T^{sup}_{DHN}} - \frac{T_0}{T_{HS}}\right) \quad (22)$$

Exergy destruction within the network's sub-stations was calculated through the difference in exergy factor of heat between the network's supply temperature and the end-user delivery temperature (eq. 23). The values assumed for these temperatures were T_{DHN}^{sup} = 85 ˚C and T_{SST}^{in} = 60 ˚C, respectively.

$$\dot{Ex}_{SST}^{D}(t) = \dot{Q}_{DHN}(t) \cdot \left(\frac{T_0}{T_{SST}^{in}} - \frac{T_0}{T_{DHN}^{sup}}\right) \quad (23)$$

The only criterion used for exergetic optimization is the global annual exergy efficiency, η_{GLOB}^{ex} (eq. 23), calculated through the ratio of global annual exergy loss $\dot{Ex}_{GLOB}^{L}$ (eq. 24) to the global annual exergy input (eq. 25).

$$\eta_{GLOB}^{ex} = 1 - \frac{\dot{Ex}_{GLOB}^{L}}{\dot{Ex}_{GLOB}^{in}} \quad (23)$$

$$\dot{Ex}_{GLOB}^{L} = \sum_{t=t_{ini}+\Delta t}^{t=t_f} \left[\dot{Ex}_{DISS}^{D}(t) + \dot{Ex}_{TES}^{l}(t) + \dot{Ex}_{HP}^{D}(t) + \dot{Ex}_{HS}^{D}(t) + \dot{Ex}_{DHN}^{D}(t) + \dot{Ex}_{SST}^{D}(t)\right] \cdot \Delta t \quad (24)$$

$$\dot{Ex}_{GLOB}^{in} = \sum_{t=t_{ini}+\Delta t}^{t=t_f} \left[\dot{Ex}_{wh}(t) + \dot{W}_{HP}^{el}(t) + \dot{Q}_{HS}(t) \cdot \left(1 - \frac{T_0}{T_{HS}}\right) \cdot \left(\frac{1}{\eta_{HS}^{ex}}\right)\right] \cdot \Delta t \quad (25)$$

3. Results and discussion

3.1. Results from the energy analysis

Figure 5 presents the evolution of the Recovery Factor (*RF*) as a function of the TES capacity, for the three possible temperatures of waste heat rejection (T_{wh}). For each temperature, the reference case (i.e. without heat valorization) is also displayed. Upon utilization of the recovery system, the *RF* increases from an obvious 0 % to considerably higher values (already between 20 % and 30 % without any storage). As a TES of greater and greater capacity is used, the RF continues to increase logically because more and more waste heat can be stored for later usage. With a TES capacity of 40 MWh, the *RF* has approximately doubled with respect to valorizing waste heat without using a TES. The recovery potential is similar to that reported in other studies on the utilization of industrial waste heat in district heating [15].

Increasing the waste heat temperature benefits the recovery of waste heat, although the reasons are different in each case. At T_{wh} = 50 ˚C, the higher COP of the heat pump implies a greater intake of waste heat, ultimately resulting in higher *RF* values. At T_{wh} = 85 ˚C, it is the absence of heat pump that forces the system to take in much more waste heat, resulting in even higher *RF* values. Based on this indicator, the optimization would suggest rejecting the LNCMI's heat at 85 ˚C and not using a heat pump at all. In this case, the WHRS would be made up of the TES only (and of course the pipelines and connections, which were neglected in this study).

The first conclusion from this figure is clear: whatever the waste heat's temperature, it is energetically interesting to use the recovery system. Between 20 % and 57 % of the waste heat can be recovered, depending on the design. The *RF* suggests a TES as large as possible, which is only partially true, as there are physical, technical and economic considerations to the optimal storage capacity [33,34]. As shown in Fig. 5, the cumulative benefits of a larger TES are asymptotic, while its investment cost probably follows a different tendency. Therefore, an energetic-economic optimum can be intuitively perceived before a capacity of 40 MWh is reached. However, given the absence of economic or technical constraints in the present model, a TES of 40 MWh is suggested as a provisory conclusion.

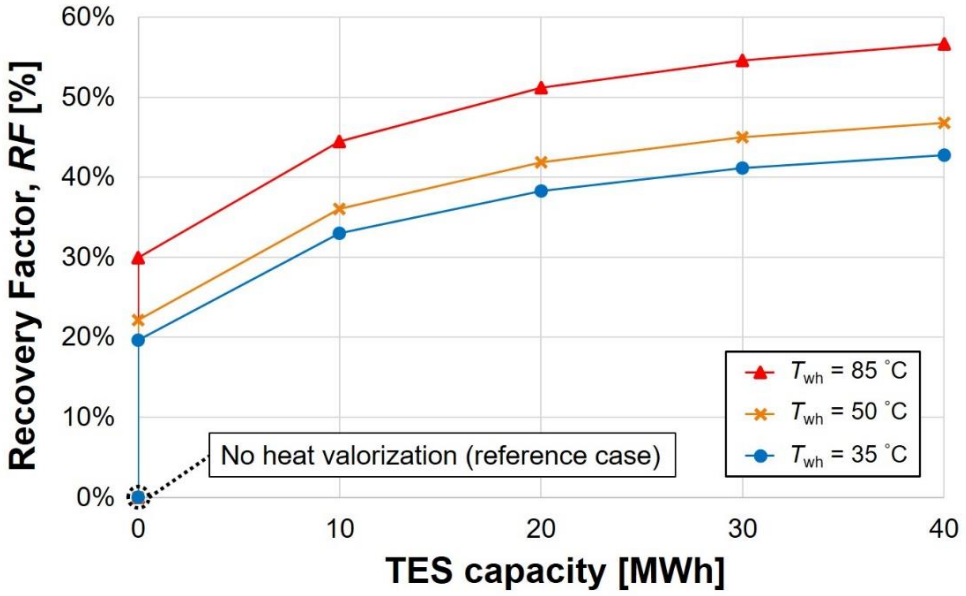

Figure 5. Recovery Factor (RF) as a function of the thermal energy storage (TES) capacity, for different waste heat temperatures.

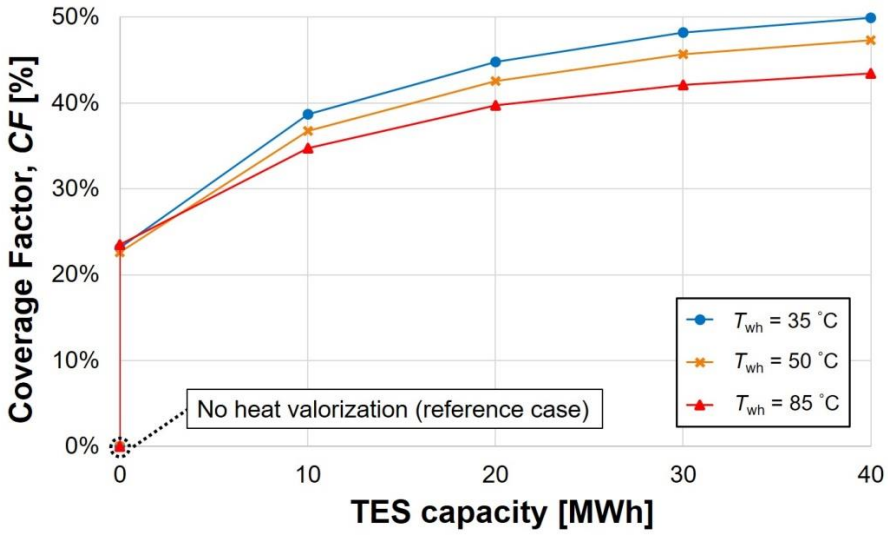

Figure 6. Coverage Factor as a function of the storage capacity, for different waste heat temperatures.

Figure 6 presents the evolution of the Coverage Factor (*CF*) as a function of the TES capacity, for the three temperatures of waste heat (T_{wh}), including reference cases. Like the previous indicator, the *CF* also shows promising results when using the WHRS, and suggests a TES as large as possible. As for the recommendation on the TES, the same economic considerations from the previous paragraph apply here.

The effect of the waste heat temperature on the *CF*, however, is inverse to its effect on the *RF*: higher T_{wh} imply a lower coverage of the residential demands. These divergences increase as the TES capacity increases. The key to explain these results is in the heat pump's COP. Indeed, in the scenario with T_{wh} = 35 ˚C the WHRS benefits from a COP = 3 of the heat pump, meaning that 2 GWh of waste heat yield 3 GWh injected to the DHN, so the ratio is $\dot{Q}_{DHN}^{in}/\dot{Q}_{wh}^{35\,^{\circ}C} = 1.5$. Meanwhile, in the scenario with T_{wh} = 85 ˚C there is no heat pump at all, which means that 1 GWh of waste heat yields 1 GWh for the DHN, so the ratio is $\dot{Q}_{DHN}^{in}/\dot{Q}_{wh}^{85\,^{\circ}C} = 1$ $Q_{in,DHN}/Q_{wh,85\ ^{\circ}C}$ = 1. The ratio is lower, that explains the lower values of *CF*.

Results with T_{wh} = 50 ˚C are both counter-intuitive and interesting. Here, the heat pump's COP is 4.29, i.e. higher than with T_{wh} = 35 ˚C (where COP = 3). So, one could think that the WHRS should be capable of covering more residential needs. However, the COP = 4.29 implies that 3.29 GWh of waste heat yield 4.29 GWh of heat injected to the DHN, giving a ratio of $\dot{Q}_{DHN}^{in}/\dot{Q}_{wh}^{50\,^{\circ}C} = 4.29\ GWh/3.29\ GWh = 1.3$, lower than with T_{wh} = 35 ˚C. We remind here that the heat pump's maximum thermal power output is the same in both scenarios (see the model description).

Therefore, with T_{wh} = 50 ˚C the heat pump gives the same maximum thermal output as with T_{wh} = 35 ˚C, but requires more waste heat to do so. So, at certain moments of the year, the latter can continue to produce heat while the former cannot. This difference would not exist if unlimited waste heat was available in both scenarios, in which case the *CF* would be exactly the same. But in reality, the waste heat is indeed limited, and in addition it is temporally mismatched with the residential demands. This reasoning explains why $CF_{T_{wh}=50\,^{\circ}C} < CF_{T_{wh}=35\,^{\circ}C}$ despite the fact that $COP_{HP}^{T_{wh}=50\,^{\circ}C} > COP_{HP}^{T_{wh}=35\,^{\circ}C}$. The classical definition of the COP was misleading for our predictions on this particular indicator, for this particular study case.

Figure 6 is rich in conclusions, especially when compared to Figure 5. Both the *RF* and the *CF* agree on the interest of the WHRS, and suggest a thermal storage unit as large as possible. Nevertheless, a different design is suggested depending on which indicator is to be maximized. The optimal source-oriented design (i.e. focused on the *RF*) would consist in rejecting waste heat at 85 ˚C and not using a heat pump at all. Such design would give the highest possible *RF* (56.7 %), but a *CF* of "only" 43.4 %. On the other hand, the optimal demand-oriented design (i.e. focused on the *CF*) would prefer rejecting waste heat at 35 ˚C and using a heat pump. This would lead to the

maximum possible *CF* (49.9 %), but a lower *RF* (42.8 %) compared to the source-oriented design. Paradoxically enough, rejecting waste heat at 50 ˚C does not seem promising for neither of the indicators, in spite of the heat pump's higher COP.

Of course, these conclusions are preliminary. As a matter of fact, energetic criteria alone are usually inconclusive when not completed by other criteria, such as economic, environmental or technical ones. Moreover, most of the indicators are sensitive to the control volume, which may be "shaped" following the interests of different parties of a same case study. Usually, the final decision in such projects requires a multi-agent approach. Without it, it is difficult to state an optimal solution not based on "biased" indicators, chosen in the best interest of only some of the parties.

In the next section, we suggest the global exergy efficiency of the DHN + WHRS system as tool for identifying the optimal design. By taking into account all local exergy destructions, this indicator aims at neither excluding, nor favoring the interests of any party (i.e. the LNCMI's owners or the DHN's owners). This evaluation of the global exergy destruction does not really have an equivalent in the first-law analysis, as energy is never destroyed. It is likewise difficult to define other indicators on a global scale, except for maybe environmental indicators.

3.2. Results from the exergy analysis

Figure 7 presents the evolution of the global annual exergetic efficiency (DHN + WHRS) as a function of the TES capacity, for the three waste heat rejection temperatures. Conversely to the *RF* and the *CF*, the exergy efficiency is not zero in the reference case. Its value (in the reference case) decreases when the waste heat temperature increases. This is due to the higher exergetic value of the waste heat that is dumped into the river. Therefore, the exergy analysis suggests to reject heat at the lowest possible temperature (35 ˚C in this study) whenever there is no heat recovery. This is already a remarkable observation, because the energetic indicators do not distinguish between different waste heat temperatures in the reference case. The *RF* and the *CF* had the same value in all scenarios.

Exergy efficiency increases upon utilization of the WHRS. With no thermal storage, the indicator still recommends rejecting heat at 35 ˚C, although differences between the three temperatures are smaller than in the reference case.

Then, as a TES of larger and larger capacity is used, the recommendations given by the indicator change. With storage capacities from 10 MWh to 40 MWh, the exergy analysis recommends T_{wh} = 85 ˚C and not using a heat pump. That is logical: because it consumes electricity, the heat pump is a large source of exergy destruction in

comparison with the direct injection of heat into the DHN (see Ex_{HP}^{D} on Table 2 for details). Exergy efficiency points out the 40 MWh storage as optimal. However, since its evolution is asymptotic like those of the *RF* and the *CF*, the aforementioned technical/economic considerations apply here as well. With the current hypotheses, rejecting at T_{wh} = 50 ˚C is not the most promising choice in any of the scenarios, for any of the indicators.

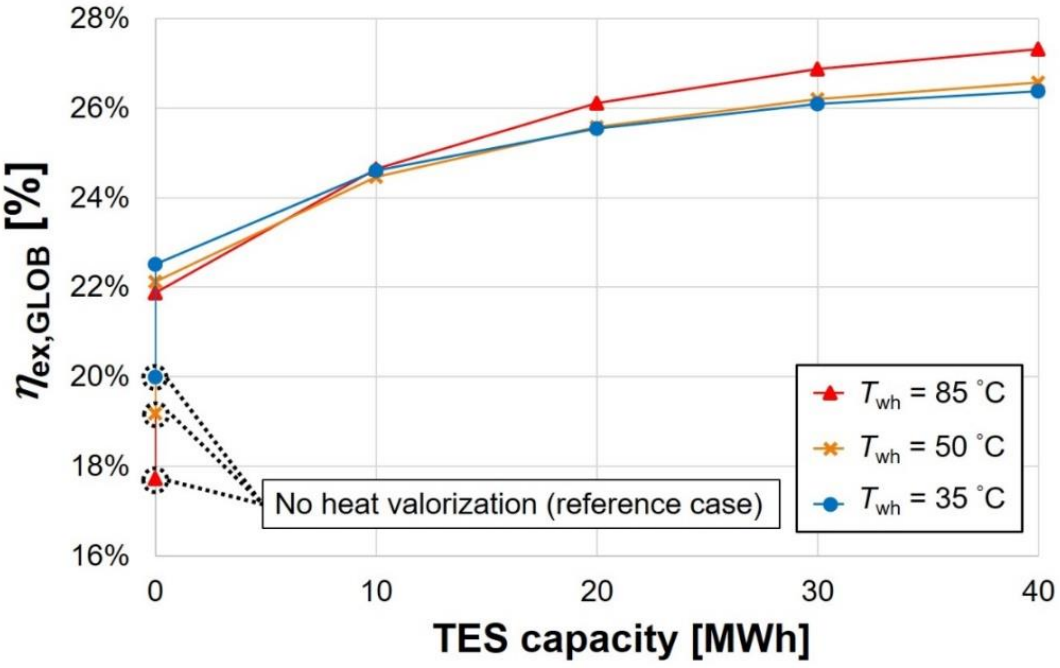

Figure 7. Global annual exergetic efficiency as a function of the storage capacity, for different waste heat temperatures.

The main conclusion from Fig. 7 is that the exergy-based optimal design for the WHRS is T_{wh} = 85 ˚C and a storage capacity of 40 MWh. This agrees with the *RF* and partially disagrees with the *CF*, which rather suggests T_{wh} = 35 ˚C and a storage capacity of 40 MWh. With all indicators considered, there exist two different optimal designs. The yearly operation of each one (with an optimal management of the WHRS) is analyzed in the next section.

Figure 8 depicts in detail the global and local exergy destructions with each T_{wh} and a 40 MWh TES, to further illustrate the effect of the rejection temperature. The very first observation is that Ex_{GLOB}^{L} is lower with than without heat recovery, in all scenarios. With heat recovery a new exergy destruction is introduced by the heat pump (Ex_{HP}^{D}), but in exchange, that of the heat supplier (Ex_{HS}^{D}) is cut back almost by half. A side benefit is the decrease in Ex_{DHN}^{D}, thanks to the lower temperature of the valorized heat (85 ˚C) with respect to the heat supplier's (120 ˚C). In sum, the added Ex_{HP}^{D} is largely compensated (refer to Table 2 for detailed results).

A subtler conclusion to draw from Fig. 8 is that rejecting heat at higher temperatures is an exergetically risky move that requires careful planning. While the potential reduction in Ex^{L}_{GLOB} seems rather modest, its potential increase is substantial in the event of a poorly monitored WHRS. Of course, the waste heat has a higher exergetic value at 50 ˚C and at 85 ˚C. If a large portion of it is dissipated: 1) the benefits of the higher T_{wh} are lost; 2) Ex^{D}_{DISS} increases notably. This is the reason why an optimal management is crucial. In fact, all results shown in this study correspond to an optimal management of the WHRS, including (and especially) the storage unit. This optimal management was found thanks to the OMEGAlpes tool, presented earlier in this article.

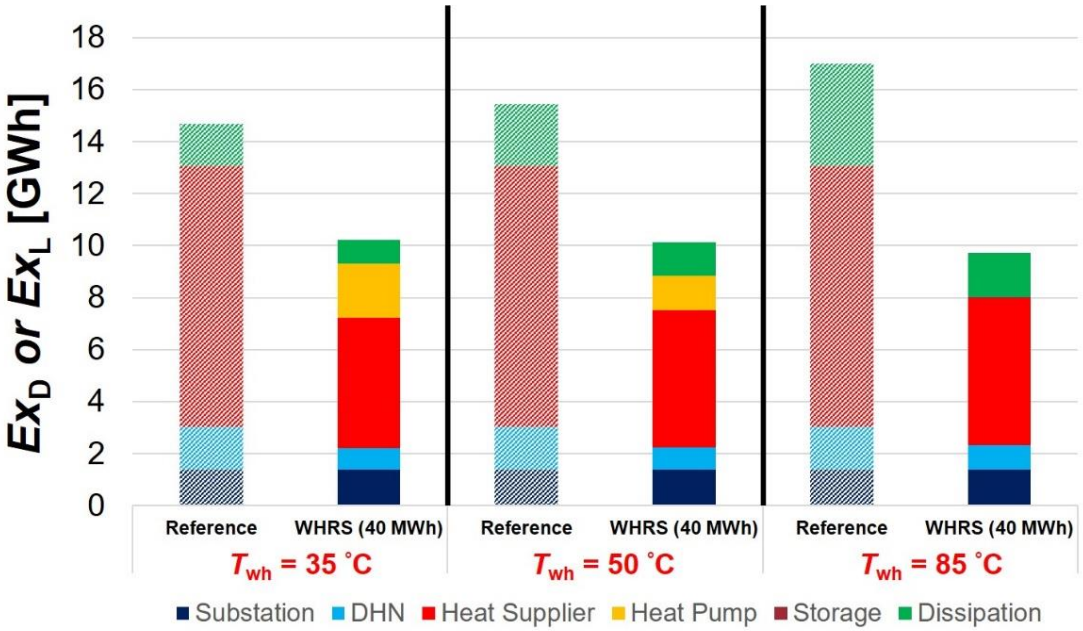

Figure 8. Local and global exergy destructions at 3 different waste heat temperatures (reference case vs valorization system with 40 MWh storage).

It would be exergetically interesting to reject at 85 ˚C whenever there is residential demand, and at 35 ˚C or lower when the waste heat is to be dissipated. This kind of "dynamic" management of T_{wh} would result in an even lower Ex^{L}_{GLOB} than that obtained in this study. Furthermore, increasing T_{wh} could lead to economic savings for the high-temperature heat supplier. It could generate benefit for the LNCMI too, as they would be able to sell their heat (be it waste or upgraded) at higher prices. An exergo-economic analysis on this decision would be interesting.

Table 2 compiles the main results for all additional scenarios considered. In addition to the three main indicators, the table shows all exergy destructions and the inlet/outlet energy flows of the heat pump. Whenever no heat pump or thermal storage is being used, the term "N/A" is displayed for all magnitudes referring to those units. In the

scenarios with T_{wh} = 85 ˚C, where there is no heat pump, the values displayed as Q_{HP}^{in} and Q_{HP}^{out} correspond to the inlet/outlet heat flows of the overall WHRS, which happen to be practically the same since heat losses at the TES are very small. These values are conveniently pointed out with an asterisk in brackets.

Table 2. Main energetic and exergetic results for every scenario in this study.

T_{wh}	Q_{TES}^{max}	Q_{HP}^{in}	W_{HP}^{el}	Q_{HP}^{out}	*RF*	*CF*	η_{GLOB}^{ex}	Ex^L *or* Ex^D **[GWh/year]**						
[˚C]	[MWh]	[GWh/y]	[GWh/y]	[GWh/y]	[%]	[%]	[%]	GLOB	DISS	TES	HP	HS	DHN	SUBS
35 (REF)	0 (w/o WHRS)	N/A	N/A	N/A	0.0	0.0	20.0	14.7	1.6	N/A	N/A	10.0	1.6	1.4
35	0 (w/ WHRS)	3.61	1.81	5.42	19.6	23.1	22.5	12.6	1.3	N/A	1.0	7.7	1.3	1.4
35	10	6.05	3.03	9.08	33.0	38.7	24.6	11.2	1.1	0.001	1.6	6.2	1.0	1.4
35	20	7.01	3.50	10.51	38.2	44.8	25.5	10.7	1.0	0.002	1.9	5.5	0.9	1.4
35	30	7.54	3.77	11.31	41.2	48.2	26.1	10.4	0.9	0.003	2.0	5.2	0.9	1.4
35	40	7.81	3.90	11.71	42.8	49.9	26.4	10.2	0.9	0.005	2.1	5.0	0.8	1.4
50 (REF)	0 (w/o WHRS)	N/A	N/A	N/A	0.0	0.0	19.2	15.4	2.4	N/A	N/A	10.0	1.6	1.4
50	0 (w/ WHRS)	4.07	1.24	5.31	22.1	22.6	22.1	12.9	1.9	N/A	0.6	7.8	1.3	1.4
50	10	6.62	2.01	8.63	36.1	36.8	24.5	11.3	1.5	0.002	1.0	6.3	1.0	1.4
50	20	7.66	2.33	9.99	41.8	42.6	25.6	10.7	1.4	0.005	1.2	5.8	0.9	1.4
50	30	8.21	2.50	10.71	45.0	45.6	26.2	10.3	1.3	0.008	1.3	5.5	0.9	1.4
50	40	8.52	2.59	11.11	46.8	47.3	26.6	10.1	1.3	0.011	1.3	5.3	0.9	1.4
85 (REF)	0 (w/o WHRS)	N/A	N/A	N/A	0.0	0.0	17.7	17.0	4.0	N/A	N/A	10.0	1.6	1.4
85	0 (w/ WHRS)	5.51 (*)	N/A	5.51 (*)	30.0	23.5	21.9	13.1	2.8	N/A	N/A	7.7	1.3	1.4
85	10	8.18 (*)	N/A	8.15 (*)	44.5	34.7	24.6	11.2	2.2	0.001	N/A	6.6	1.1	1.4
85	20	9.41 (*)	N/A	9.32 (*)	51.2	39.7	26.1	10.4	1.9	0.020	N/A	6.0	1.0	1.4
85	30	10.04 (*)	N/A	9.88 (*)	54.6	42.1	26.9	10.0	1.8	0.034	N/A	5.8	0.9	1.4
85	40	10.42 (*)	N/A	10.19 (*)	56.7	43.4	27.3	9.8	1.7	0.049	N/A	5.7	0.9	1.4

(*) In this scenario there is no heat pump. The values shown correspond to the inlet and outlet of the WHRS.

3.3. Analysis of the optimal yearly operation with the energy- and exergy-based optimal designs

After the energy and exergy analyses, two different optimal designs have been identified for the WHRS. The demand-oriented energy-based optimization recommends rejecting waste heat at T_{wh} = 35 ˚C and a WHRS consisting of a heat pump and a 40 MWh TES. On the other hand, both the exergy-based and the source-oriented energy-based optimizations suggest T_{wh} = 85 ˚C, a 40 MWh storage, and no heat pump at all. In this section, the Sankey and Grassman diagrams show, respectively, the annual energy and exergy flows of the optimized operation in both designs.

Figures 9a and 9b correspond to the design with $Q_{TES}^{max} = 40\ MWh$, T_{wh} = 35 ˚C and a heat pump being used. Yellow represents heat flows at 35 ˚C, orange those at 85 ˚C or lower, and red those over 85 ˚C. Electric flows are depicted

365 in dark purple, and the primary products for the combustion process of the heat supplier are depicted in green,
366 somehow representing chemical exergy. On the Grassman diagrams, exergy destruction within each unit is
367 represented by a black triangle on the upper-right corner, with the value displayed in white and in brackets. For an
368 easier interpretation of the diagram, the calculation of the global annual exergy loss and efficiency is also
369 displayed.

370

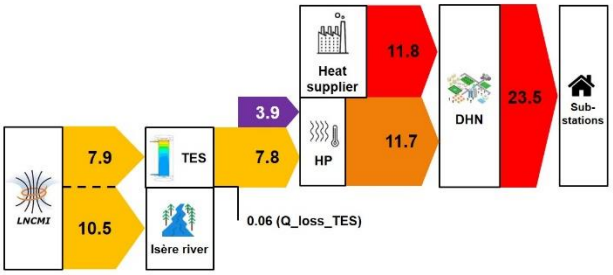

Figure 9a. Sankey diagram (energy flows in GWh/year) for the optimal operation of the WHRS with an energy-based, demand-oriented optimal design (i.e. waste heat at 35 °C, and a heat pump).

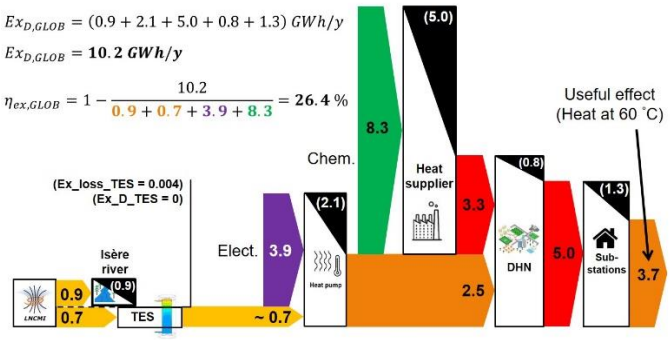

Figure 9b. Grassman diagram (exergy flows in GWh/year) for the optimized operation of the WHRS with an energy-based, demand-oriented optimal design (i.e. waste heat at 35 °C, and a heat pump).

371

372 Two interesting reflections emerge from comparing the Sankey and Grassman diagrams. First, the notable
373 difference in quality between electrical energy (exergy factor of 1) and thermal energy. Second, the difference in
374 quality between thermal flows at different temperatures. Note how the electricity consumed by the heat pump is the
375 smallest energy flow (Sankey), but in exergy, it is greater than most of the thermal flows (Grassman). Note also
376 how the heat pump and the heat supplier deliver almost the same amount of energy, but in exergy they are clearly
377 different (2.5 GWh in front of 3.3 GWh). This is due to the temperature difference (85 ˚C in front of 120 ˚C).

378 Figures 10a and 10b correspond to the design with $Q_{TES}^{max} = 40\ MWh$, T_{wh} = 85 ˚C and no heat pump at all. These
379 diagrams follow the same color code as the previous ones. Note how in both Sankey diagrams (Figs. 8a and 9a)
380 the amount of waste heat is the same, and the residential demand too (23.5 GWh/year). The differences are in the
381 intermediary management, being the absence of heat pump in Fig. 9a the most noticeable difference.

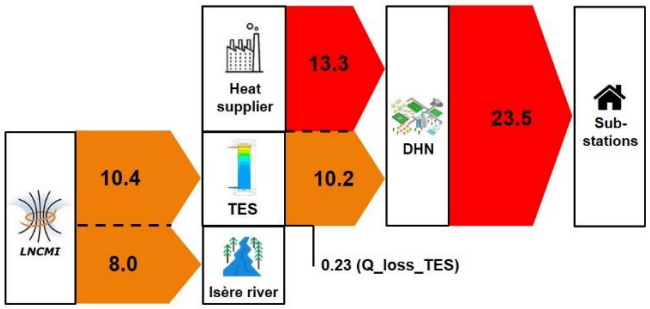

Figure 10a. Sankey diagram (energy flows in GWh/year) for the optimized operation of the WHRS with a source-oriented, energy-based optimal design (i.e. waste heat at 85 °C, and no heat pump). This design is also supported by the exergy-based optimization.

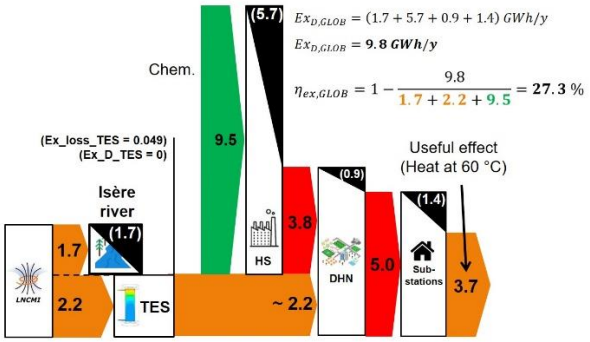

Figure 10b. Grassman diagram (exergy flows in GWh/year) for the optimal operation of the WHRS with a source-oriented, energy-based design (i.e. waste heat at 85 °C, and no heat pump). This design is also supported by the exergy-based optimization.

Since the design of the WHRS is completely different in Figs. 9 and 10, there is no point in trying to establish a quantitative comparison between the Sankey diagrams. As for the Grassman diagrams, it can be stated that the design in Fig. 10b increases global annual exergy efficiency (η^{ex}_{GLOB} = 27.3 %) with respect to the design in Fig. 9b (η^{ex}_{GLOB} = 26.4 %). Note that this is thanks to the absence of heat pump, in which electricity is transformed into heat.

Interestingly enough, note how in both scenarios the heat pump has the second highest exergy destruction, only surpassed by the combustion process of the heat supplier, which transforms chemical exergy into thermal exergy. The non-thermal-to-thermal units show the highest irreversibilities, while the thermal-to-thermal units show the lowest. Perhaps a conclusion would be that it is exergetically wise to meet thermal demands with purely thermal sources, avoiding energy transformation as much as possible. However, this conclusion is hardly generalizable from these results alone.

4. Conclusions and perspectives

This article presented an analysis and comparison between an energy-based and an exergy-based optimal design of a waste heat recovery system for district heating. The energy-based analysis used a demand-oriented indicator (heating demand coverage) and a source-oriented indicator (waste heat recovered). The exergy-based analysis used the global annual exergy efficiency as the only indicator. The study considered three waste heat temperatures (35 ˚C, 50 ˚C and 85 ˚C), and five storage capacities (from 0 MWh to 40 MWh in steps of 10 MWh). Each design option was simulated by means of the yearly profiles and optimized through mixed-integer linear programming and a specialized open-source tool called OMEGAlpes.

The three indicators agree on the interest of recovering waste heat. Their values improve in an asymptotic tendency if the storage capacity is increased. The three indicators recommend the highest analyzed storage capacity (40 MWh), although economic considerations would most likely alter this conclusion. In addition, the indicators differ in the optimal design that they suggest. The energy-based, demand-oriented optimization recommends rejecting waste heat at 35 ˚C and valorizing it with a heat pump and a 40 MWh thermal storage. This design leads to the maximum possible demand Coverage Factor of *CF* = 49 %. On the other hand, both the exergy-based and the source-oriented energy-based optimizations agree on a different design. They suggest rejecting waste heat at 85 ˚C and using a 40 MWh storage, with no heat pump at all. This other design would maximize the recovery of waste heat (*RF* = 55 %) and the global annual exergy efficiency (η_{GLOB}^{ex} = 27 %). The yearly operation of both optimal designs (with an optimal management of the storage unit) was analyzed by means of the Sankey and Grassman diagrams.

Most of the results from this study are to be completed by additional criteria (economic, environmental, technical…). For instance, both the energy and the exergy analyses suggest a storage system as large as possible, but economy and the technical constraints would lead to a compromise. Moreover, the exergy analysis suggests that rejecting waste heat at higher temperatures is slightly favorable, but risky if the recovery system is not managed optimally. Nevertheless, waste heat is generally low-cost, while capital gains/savings in other units can be high. Therefore, an exergo-economic analysis might reinforce the interest of this strategy and mitigate its risk.

These considerations are an opening for a future study comparing the energy and exergy analyses to their economic counterparts. Such a study could: 1) Determine the definitive optimal storage capacity; 2) Confirm the interest of waste heat at higher temperatures; 3) Emphasize the differences between energy- and exergy-based optimizations.

A storage unit is not the only way to cope with an energy mismatch. In this particular study case, the LNCMI's annual calendar of experiments could be re-adjusted to better fit the residential demand curve. Such scenario deserves a thorough economic analysis, as the optimal response is not obvious. The new calendar should prioritize experiments in winter, where most of the residential needs take place. However, electricity prices are higher in winter. This scenario would only be feasible if the LNCMI's gains from selling waste heat could outweigh the higher expenses in electricity consumption. This perspective is currently under consideration by the LNCMI's engineering team. Furthermore, demand-side management (DSM) approaches are other ways to be studied in order to adapt

the consumption profile to the available waste heat. Once again, these approaches need to include economic aspects, such as the contracts between the supplier and the end-users.

Another interesting perspective comes from the LNCMI's side, too. As a matter of fact, the temperature of heat rejection can be adjusted by managing their cooling loop (hydraulic pumps' rotational speed, etc.). This cooling loop could be dynamically controlled to target an optimal match with the residential demands. Such a dynamic control would adjust for higher temperatures when the experiments and the residential needs are simultaneous, and lower temperatures when they are not. This strategy might improve the results of the exergetic analysis.

Acknowledgement

The authors are grateful to La Région Auvergne-Rhône-Alpes for their financial support through the OREBE projet (Optimisation holistique des Réseaux d'Energie et des Bâtiments producteurs d'énergies dans les Eco-quartiers). They are also grateful to the ADEME (the French Agency for Environment and Energy Management) for their financial support through the RETHINE project (Réseaux Electriques et THermiques InterconNEctés). This work has been partially supported by the CDP Eco-SESA receiving fund from the French National Research Agency in the framework of the "Investissements d'avenir" program (ANR-15-IDEX-02).

The authors thank the other members of the developer team of the optimization tool used in this study, OMEGAlpes, especially Camille Pajot (G2Elab, Grenoble), Benoit Delinchant (G2Elab, Grenoble) and Lou Morriet (G2Elab and PACTE, Grenoble).

References

[1] Lund H, Werner S, Wiltshire R, Svendsen S, Thorsen JE, Hvelplund F, et al. 4th Generation District Heating (4GDH) - Integrating smart thermal grids into future sustainable energy systems. Energy 2014;68:1–11. doi:10.1016/j.energy.2014.02.089.

[2] Rezaie B, Rosen MA. District heating and cooling : Review of technology and potential enhancements. Appl Energy 2012;93:2–10. doi:10.1016/j.apenergy.2011.04.020.

[3] Svensson IL, Jönsson J, Berntsson T, Moshfegh B. Excess heat from kraft pulp mills: Trade-offs between internal and external use in the case of Sweden-Part 1: Methodology. Energy Policy 2008;36:4178–85. doi:10.1016/j.enpol.2008.07.017.

[4] Solheimslid T, Harneshaug HK, Lümmen N. Calculation of first-law and second-law-efficiency of a Norwegian combined heat and power facility driven by municipal waste incineration-A case study. Energy Convers Manag 2015;95:149–59. doi:10.1016/j.enconman.2015.02.026.

[5] Sangi R, Müller D. A novel hybrid agent-based model predictive control for advanced building energy systems. Energy Convers Manag

2018;178:415–27. doi:10.1016/j.enconman.2018.08.111.

[6] Bejan A, Tsatsaronis G, Moran M. Thermal Design and Optimization. 1st ed. Canada: John Wiley & Sons; 1996.

[7] Terehovics E, Veidenbergs I, Blumberga D. Exergy Analysis for District Heating Network. Energy Procedia 2017;113:189–93. doi:10.1016/j.egypro.2017.04.053.

[8] Gong M, Werner S. Exergy analysis of network temperature levels in Swedish and Danish district heating systems. Renew Energy 2015;84:106–13. doi:10.1016/j.renene.2015.06.001.

[9] Kilkiş Ş. A net-zero building application and its role in exergy-aware local energy strategies for sustainability. Energy Convers Manag 2012;63:208–17. doi:10.1016/j.enconman.2012.02.029.

[10] Kilkiş Ş. Energy system analysis of a pilot net-zero exergy district. Energy Convers Manag 2014;87:1077–92. doi:10.1016/j.enconman.2014.05.014.

[11] Leduc WRWA, Van Kann FMG. Spatial planning based on urban energy harvesting toward productive urban regions. J Clean Prod 2013;39:180–90. doi:10.1016/j.jclepro.2012.09.014.

[12] Keçebaş A, Yabanova I. Economic analysis of exergy efficiency based control strategy for geothermal district heating system. Energy Convers Manag 2013;73:1–9. doi:10.1016/j.enconman.2013.03.036.

[13] Li H, Svendsen S. Exergy and energy analysis of low temperature district heating network. Energy 2012;45:237. doi:10.1016/j.energy.2012.03.056.

[14] Cao S, Sirén K. Matching indices taking the dynamic hybrid electrical and thermal grids information into account for the decision-making of nZEB on-site renewable energy systems. Energy Convers Manag 2015;101:423–41. doi:10.1016/j.enconman.2015.05.053.

[15] Cooper SJG, Hammond GP, Norman JB. Potential for use of heat rejected from industry in district heating networks, GB perspective. J Energy Inst 2016;89:57–69. doi:10.1016/j.joei.2015.01.010.

[16] Cao S, Hasan A, Sirén K. On-site energy matching indices for buildings with energy conversion, storage and hybrid grid connections. Energy Build 2013;64:423–38. doi:10.1016/j.enbuild.2013.05.030.

[17] Abdoly MA, Rapp D. Theoretical and experimental studies of stratified thermocline storage of hot water. Energy Convers Manag 1982;22:275–85. doi:10.1016/0196-8904(82)90053-X.

[18] Mostafavi Tehrani SS, Saffar-Avval M, Behboodi Kalhori S, Mansoori Z, Sharif M. Hourly energy analysis and feasibility study of employing a thermocline TES system for an integrated CHP and DH network. Energy Convers Manag 2013;68:281–92. doi:10.1016/j.enconman.2013.01.020.

[19] Hodencq S, Debray F, Trophime C, Vincent B, Stutz B, Delinchant B, et al. Thermohydraulics of High Field Magnets : from microns to urban community scale. 24ème Congrès Français de Mécanique, Brest (France): 2019.

[20] Pajot C. OMEGAlpes : Outil d'aide à la décision pour une planification énergétique multi-fluides optimale à l'échelle des quartiers. Doctoral Thesis. Université de Grenoble (France), 2019.

[21] Pajot C, Morriet L, Hodencq S, Delinchant B, Wurtz F, Reinbold V, et al. An Optimization Modeler as an Efficient Tool for Design and Operation for City Energy Stakeholders and Decision Makers To cite this version : HAL Id : hal-02285954. 16th IBPSA Int. Conf., Rome (Italy): 2019.

[22] Morriet L, Pajot C, Delinchant B, Marechal Y, Wurtz F, Debray F, et al. Optimisation multi-acteurs appliquée à la valorisation de chaleur

fatale d ' un acteur industriel flexible. Conférence Francoph. l'International Build. Perform. Simul. Assoc. Garantie performances., 2018.

[23] Olsthoorn D, Haghighat F, Mirzaei PA. Integration of storage and renewable energy into district heating systems : A review of modelling and optimization. Sol Energy 2016;136:49–64. doi:10.1016/j.solener.2016.06.054.

[24] Allegrini J, Orehounig K, Mavromatidis G, Ruesch F, Dorer V, Evins R. A review of modelling approaches and tools for the simulation of district-scale energy systems. Renew Sustain Energy Rev 2015;52:1391–404. doi:10.1016/j.rser.2015.07.123.

[25] Delinchant B, Hodencq S, Maréchal Y, Morriet L, Pajot C, Reinbold V, et al. OMEGAlpes examples. https://gricad-gitlab.univ-grenoble-alpes.fr/omegalpes/omegalpes_examples.

[26] Delinchant B, Hodencq S, Maréchal Y, Morriet L, Pajot C, Reinbold V, et al. OMEGAlpes documentation. Univ Grenoble Alpes, CNRS, Grenoble INP, G2Elab, CEA, Univ Paris-Sud. https://omegalpes.readthedocs.io/en/latest/.

[27] Verda V, Colella F. Primary energy savings through thermal storage in district heating networks. Energy 2011;36:4278–86. doi:10.1016/j.energy.2011.04.015.

[28] Mouret S, Chammas M, Attard P, De Bucy J, Lochmann H, Le Gars L, et al. Étude de valorisation du stockage thermique et du power-to-heat. ADEME/ATTE, France: 2016.

[29] Cao S, Hasan A, Sirén K. Matching analysis for on-site hybrid renewable energy systems of office buildings with extended indices. Appl Energy 2014;113:230–47. doi:10.1016/j.apenergy.2013.07.031.

[30] Pons M. On the reference state for exergy when ambient temperature fluctuates. Int J Thermodyn 2009;12:113–21.

[31] Terhan M, Comakli K. Energy and exergy analyses of natural gas-fired boilers in a district heating system. Appl Therm Eng 2017;121:380–7. doi:10.1016/j.applthermaleng.2017.04.091.

[32] Vučković GD, Stojiljković MM, Vukić M V. First and second level of exergy destruction splitting in advanced exergy analysis for an existing boiler. Energy Convers Manag 2015;104:8–16. doi:10.1016/j.enconman.2015.06.001.

[33] Fasquelle T, Falcoz Q, Neveu P, Hoffmann JF. Numerical simulation of a 50 MWe parabolic trough power plant integrating a thermocline storage tank. Energy Convers Manag 2018;172:9–20. doi:10.1016/j.enconman.2018.07.006.

[34] Hoffmann JF, Fasquelle T, Goetz V, Py X. Experimental and numerical investigation of a thermocline thermal energy storage tank. Appl Therm Eng 2017;114:896–904. doi:10.1016/j.applthermaleng.2016.12.053.